Hindawi
Mathematical Problems in Engineering
Volume 2018, Article ID 1890426, 9 pages
https://doi.org/10.1155/2018/1890426

Research Article

Influence of Seeker Disturbance Rejection and Radome Error on the Lyapunov Stability of Guidance Systems

Kaiwei Chen,[1] **Qunli Xia**,[1] **Xiao Du**,[2] **and Yuemin Yao**[3]

[1]*School of Aerospace Engineering, Beijing Institute of Technology, Beijing 100081, China*
[2]*China Academy of Launch Vehicle Technology, Beijing 100076, China*
[3]*Beijing Institute of Space Long March Vehicle, Beijing 100076, China*

Correspondence should be addressed to Kaiwei Chen; kwillchan@outlook.com

Received 18 March 2018; Accepted 15 May 2018; Published 20 June 2018

Academic Editor: Calogero Orlando

This study analyzes the effects of disturbance rejection and radome error on the stability of guidance systems. First, disturbance rejection rate transfer function (DRRTF) models are established. Second, the Lyapunov stability of a proportional navigation guidance system is proposed. The passivity theorems are introduced for the analysis of the Lyapunov stability of the nonlinear time-varying system. Finally, the influence of the different DRRTF models on the stability of the guidance system is analyzed by mathematical simulations. The simulation results indicate that the stable boundary of the guidance system varies and its tolerance to disturbance differs significantly for various disturbance torque types and radome slope.

1. Introduction

The stabilized platform of a gimbaled seeker isolates the body motion caused by missile maneuvering and vibration during flight. However, the isolation is incomplete due to wire pulling inside the seeker and friction among components. Consequently, missile disturbance coupling enters the seeker, thereby affecting the accuracy of the seeker output [1–3] and leading to the disturbance rejection effect. The seeker disturbance rejection effect then forms a parasitic loop within the missile guidance loop, that is, the disturbance rejection rate parasitic loop (DRRPL).

Radomes are attached to the nose of radar homing missiles. The refraction of the electromagnetic wave by the radome causes an error in the line-of-sight (LOS) angle, that is, the radome refraction angle, which also creates a parasitic loop with the guidance homing loop. In certain situations, the disturbance rejection and radome error act to reduce the stability of the guidance system and cause an increase in miss distance [4–7].

Several stability analysis approaches for guidance systems have been suggested in the literature.

(1) The first and most commonly used approach is based on the "frozen time" assumption, transforming the guidance system into a time-invariant system and analyzing the stability by the Routh criterion [8–11]. However, when the distance between the missile and the target is short or the dynamics of the guidance system are relatively fast, the "frozen time" assumption is no longer valid. Moreover, applying the Routh criterion to analyze the stability generates a large error.

(2) The second approach assumes that the terminal guidance time is infinite and uses the stability analysis method of time-varying systems on the basis of infinite time, such as the Popov and circle criteria [4, 12, 13]. These stability conditions are defined over an infinite-horizon time domain and thus are not suitable for the stability analysis of a homing guidance loop, which is only defined over a finite time interval.

(3) The third approach analyzes stability by using the finite time stability theory of time-varying systems [14–17]. This approach is practical in real engagement.

This study evaluates the Lyapunov stability over a finite time interval on the basis of the linearized model of the proportional navigation (PN) guidance system. The disturbance rejection rate is the transfer function which represents the incorrect angular rate caused by an attitude disturbance applied to the missile's body [18]. Therefore, this study

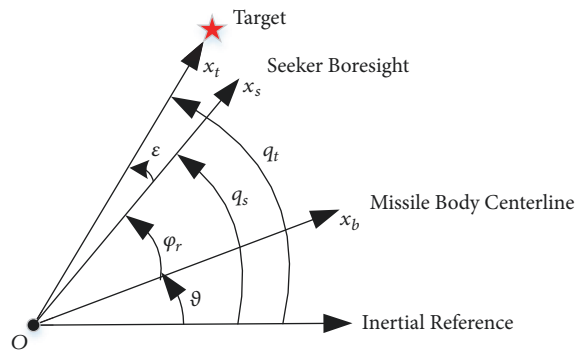

Figure 1: Basic geometry in pitch plane.

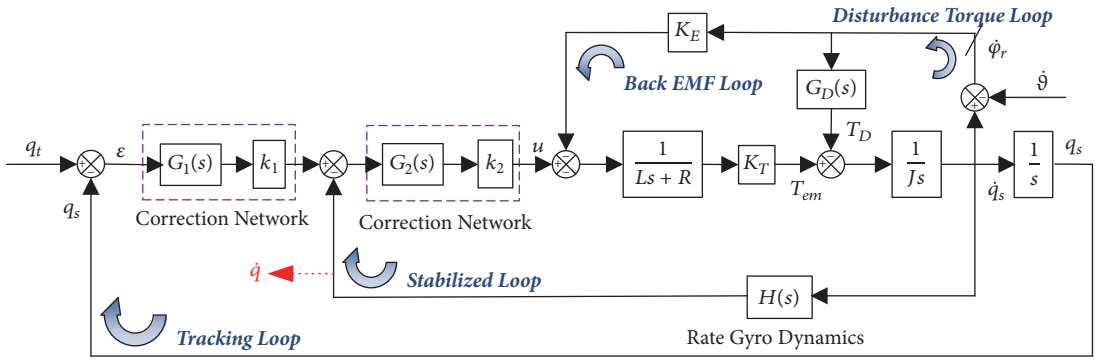

Figure 2: Control loop model of a gimbaled seeker.

establishes the disturbance rejection rate transfer function (DRRTF) models under the joint action of the disturbance torque and the radome error. A PN guidance system model is established on the basis of DRRTF. The passivity theorems for analyzing the Lyapunov stability of nonlinear time-varying systems are convenient for engineering application because they do not need to build the state space models and construct Lyapunov functions [19–21]. Therefore, this study analyzes the Lyapunov stability of the PN guidance system on the basis of the passivity theorems.

This paper is structured as follows. Section 2 establishes the DRRTF and PN guidance system models, which consider the different disturbance torque types and radome error slope. Section 3 defines the uniform asymptotical stability of the PN guidance system and introduces the Lyapunov stability represented by passivity theorems. Section 4 analyzes the stability of the PN guidance system on the basis of passivity theorems. Section 5 investigates the influence of spring torque, damping torque, and radome error slope on the Lyapunov stability of the PN guidance system by simulations. Section 6 concludes this paper.

2. Problem Formulation

2.1. Modeling of the DRRTF. Figure 1 shows the basic geometry in pitch plane. In Figure 1, q_t represents the LOS angle, q_s is the seeker rotation angle, ϑ denotes the missile attitude angle, φ_r refers to the gimbal angle, and ε stands for the seeker LOS error angle. From geometry, the detector error angle can be written as follows:

$$\varepsilon = q_t - q_s \tag{1}$$

Figure 2 presents a typical control loop model of a gimbaled seeker.

In Figure 2, L is the inductance of armature winding, R denotes the total resistance, K_T represents the torque constant, K_E stands for the back electromotive force (EMF), $T_{em}(t)$ refers to the electromagnetic torque, T_D signifies the total load torque of the motor and load, J indicates the total motor rotational inertia, and $\dot{q}$ symbolizes the LOS rate required for guidance.

Figure 2 shows that the model mainly includes the stabilized, tracking, disturbance torque, and back EMF loops. The disturbance torque loop is caused by wire pulling and friction among rotation joints, which happens in the seeker rotation process. In Figure 2, various types of disturbance torque are equivalent to the transfer function $G_D(s)$. The disturbance torque is the main factor leading to problems of the disturbance rejection rate of the gimbaled seeker, including the spring and damping torques. A real gimbaled seeker disturbance torque is a nonlinear model. A simplified model is adopted to analyze the influence of disturbance torque on seeker disturbance rejection rate and output accuracy. The expression is as follows [22]:

$$G_D(s) = \frac{K_n}{s} + K_\omega, \tag{2}$$

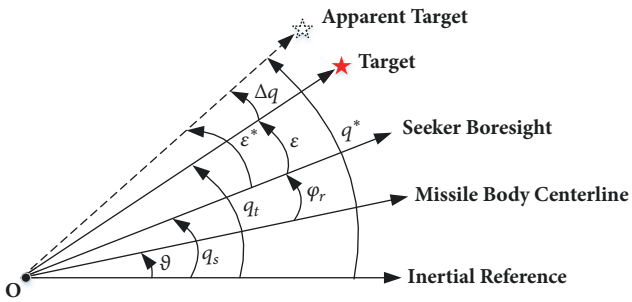

FIGURE 3: Basic geometry for radome analysis.

where K_n is the spring torque coefficient and K_ω denotes the damping torque coefficient.

The occurrence of the disturbance torque couples the missile and seeker motions, thereby causing DRRPL and reducing the accuracy of seeker control. The DRRTF $R(s)$ is defined as follows:

$$R(s) = \frac{\Delta\dot{q}(s)}{\dot{\vartheta}(s)}, \tag{3}$$

where $\Delta\dot{q}(s)$ is the additional rotation angular rate of the platform caused by the missile motion in relation to the inertial space. From the definition, the smaller the amplitude of $R(s)$, the stronger the seeker's isolation capability to the disturbance of the missile.

In accordance with Figure 2, assuming $H(s) = 1$ and ignoring the effect of back EMF, the seeker DRRTF can be educed as

$$R(s) = \frac{\Delta\dot{q}(s)}{\dot{\vartheta}(s)} = \frac{sG_D(s)(Ls+R)}{s\left[Js(Ls+R) + G_D(s)(Ls+R) + G_2(s)k_2K_T\right] + G_1(s)G_2(s)k_1k_2K_T} \tag{4}$$

With the damping torque $G_D(s) = K_\omega$ and spring torque $G_D(s) = K_n/s$ models substituted into (4), the DRRTF models under the effect of the damping and spring torques are shown in

$$R_v(s) = \frac{\Delta\dot{q}_v(s)}{\dot{\vartheta}(s)} = \frac{sK_\omega(Ls+R)}{s\left[Js(Ls+R) + K_\omega(Ls+R) + G_2(s)k_2K_T\right] + G_1(s)G_2(s)k_1k_2K_T} \tag{5}$$

$$R_s(s) = \frac{\Delta\dot{q}_s(s)}{\dot{\vartheta}(s)} = \frac{K_n(Ls+R)}{s\left[Js(Ls+R) + G_2(s)k_2K_T\right] + K_n(Ls+R) + G_1(s)G_2(s)k_1k_2K_T} \tag{6}$$

2.2. Radome Parasitic Effects in a Stabilized Seeker. The existence of radome affects the seeker measurement on the real target position. Figure 3 shows the basic missile–target geometry under the existence of the radome error.

In Figure 3, Δq denotes the radome refraction angle, ε^* is the error angle between the seeker centerline and apparent LOS, and q^* represents the apparent LOS angle caused by the radome error.

The refraction angle Δq varies with the seeker gimbal angle φ_r. For preliminary analysis, the refraction angle is assumed to be linearly proportional to the gimbal angle

$$\Delta q = R_{dom}\varphi_r, \tag{7}$$

where R_{dom} is the radome slope. R_{dom} is generally regarded as a constant despite being variable during flight [23, 24].

In accordance with the angular relationships in Figure 3, q^* can be expressed as follows:

$$q^* = q_t + (q_s - \vartheta)R_{dom}. \tag{8}$$

Considering a stable seeker tracking, ε is generally a small parameter. Thus, $q_s \approx q_t$. Then, (8) can be rewritten as follows:

$$q^* \cong q_t + (q_t - \vartheta)R_{dom} = q_t(1+R) - \vartheta R_{dom}. \tag{9}$$

Generally speaking, $R_{dom} \ll 1$. Hence, (9) can be simplified into

$$q^* = q_t - \vartheta R_{dom}. \tag{10}$$

Equation (10) shows that missile attitude is fed back to the seeker due to the existence of radome error, thereby generating a measurement error of q_t. Consequently, a radome error parasitic loop is formed in the guidance loop.

The influence of the correction network on DRRTF characteristics fluctuates on a small scale within the common operating frequencies of the seeker (less than 5 Hz), thereby failing to transform its basic amplitude-phase characteristics. Therefore, the analysis model of the disturbance rejection rate can be simplified to demonstrate intuitively its influence on the guidance and control system. Ignoring the impact of time delay process, the correction network, effect of back EMF, high-frequency dynamics, and small quantity and assuming $G_1(s) = 1$, $G_2(s) = 1$, $R \approx 1$, and $L \approx 0$, the equivalent gain of the stabilized loop is determined to be $K_2 = G_2k_2K_T/J$. In addition, the equivalent gain of the tracking loop is $K_1 = G_1k_1$. Figure 4 presents the educed seeker model with radome effects.

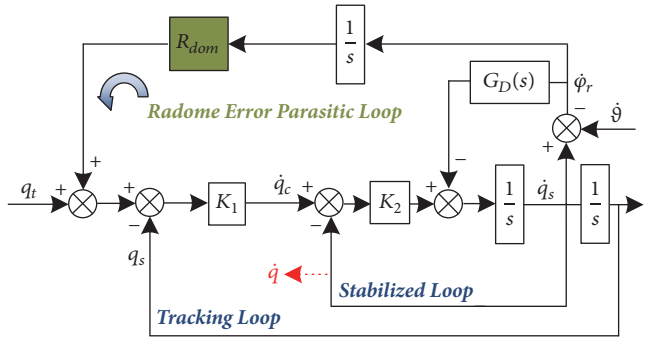

Figure 4: Simplified seeker model with radome effects.

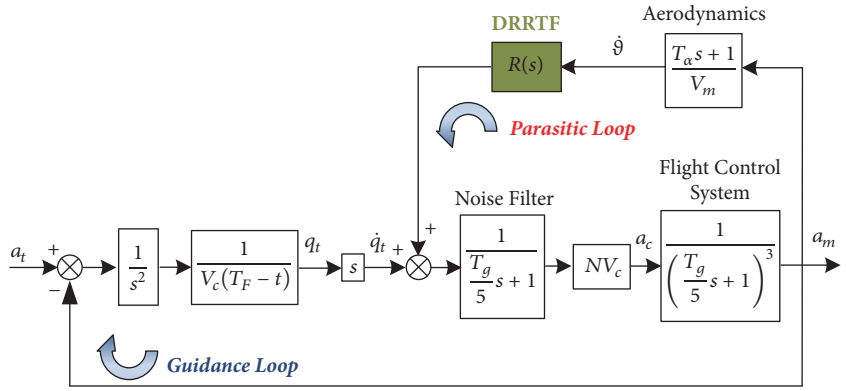

Figure 5: Guidance system model with parasitic effects.

Table 1: First-order DRRTF.

Disturbance type	DRRTF	Equivalent coefficient
Spring torque	$R_s(s) = \frac{K_s - K_r}{T_s s + 1}$	$K_s = \frac{K_n}{K_1 K_2}$
Damping torque	$R_v(s) = \frac{sK_v - K_r}{T_s s + 1}$	$K_v = \frac{K_\omega}{K_1 K_2}$

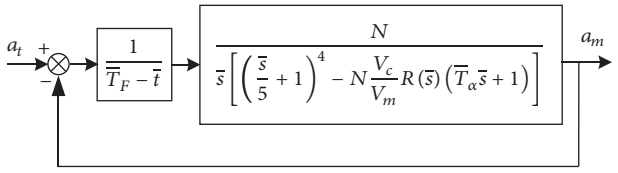

Figure 6: Dimensionless guidance system model.

Figure 4 shows that the DRRTF, including the radome slope, can be educed as (11) with $K_r = R_{dom}/(1 - R_{dom})$.

$$R(s) = \frac{\Delta\dot{q}(s)}{\dot{\vartheta}(s)} = \frac{-K_r + sG_D(s)/K_1K_2}{(1/K_1K_2)s^2 + ((G_D(s) + K_2)/K_1K_2)s + 1} \quad (11)$$

$K_1K_2 \gg K_n$ is observed when the time delay process and correction network are ignored. To simplify the analysis, on the basis of the seeker control system performance and ignoring the high-frequency dynamics, the DRRTF under the effect of both radome slope and different types of disturbance torque can be simplified as a first-order model, as shown in Table 1, where T_s is the equivalent time constant.

2.3. Guidance System Model. Figure 5 presents a block diagram of the guidance loop with the disturbance rejection and radome parasitic loop. The noise filter is considered a first-order model, the flight control system a third-order model, and the seeker dynamics a first-order model with the equivalent time constant of $T_s = T_g/5$.

In Figure 5, a_t is the target acceleration, a_m denotes the missile acceleration, V_c represents the closing velocity, V_m stands for the missile velocity, $T_F - t$ signifies the time to go, T_g refers to the guidance time constant, T_α indicates the missile turning rate time constant, and N symbolizes the effective navigation ratio of the proportional guidance.

The dimensionless method is adopted to reduce the parameter. Assuming $s = \overline{s}/T_g$, $\overline{T}_F = T_F/T_g$, $\overline{t} = t/T_g$, and $\overline{T}_\alpha = T_\alpha/T_g$, the equivalent model of the dimensionless guidance system can be obtained as shown in Figure 6.

3. Lyapunov Stability of the Guidance System

3.1. Uniform Asymptotic Stability of the Guidance System. The guidance system shown in Figure 6 is a linear time-varying

system. In this study, passivity theorems are used to analyze the Lyapunov stability of the equilibrium point of the system. When studying the Lyapunov stability, we consider the case of zero input. Let the reference input a_t in Figure 6 be zero, and the guidance system is considered as follows:

$$\dot{x} = f(t, x). \tag{12}$$

If

$$f(t, 0) = 0, \quad \forall t \geq 0, \tag{13}$$

then the origin is the equilibrium point of (12) at $t = 0$. The equilibrium point $x = 0$ of the system (12) is

(i) uniformly stable if each $\xi > 0$ has $\delta = \delta(\xi) > 0$ independent of t_0 such that

$$\|x(t_0)\| < \delta \Longrightarrow \|x(t)\| < \xi, \quad \forall t \geq t_0 \geq 0 \text{ and} \tag{14}$$

(ii) uniformly asymptotically stable if it is uniformly stable and has a positive constant c independent of t_0 such that for all $\|x(t_0)\| < c$, $x(t) \to 0$ as $t \to \infty$, uniformly in t_0; that is, for each $\eta > 0$, $T = T(\eta) > 0$ is observed, such that

$$\|x(t)\| < \eta, \quad \forall t \geq t_0 + T(\eta), \ \forall \|x(t_0)\| < c. \tag{15}$$

Therefore, if the guidance system is uniformly asymptotically stable at some initial moment t_0, then the system has Lyapunov stability at all t_0 in the defined interval and the convergence of the system will not deteriorate with an increase in t_0.

3.2. Lyapunov Stability Represented by Passivity Theorems. Passivity theorems involve the concepts of passivity and positive real. The definitions of passivity and positive real are provided in the following. Proof of the relevant lemma and theorem is presented in [19].

3.2.1. Passivity of a Time-Varying Memoryless Function. When the output of the system is independent of the state variables, the system can be expressed as $y = h(t, u)$, that is, a memoryless function. If h is a scalar function that satisfies the inequality

$$\alpha u^2 \leq uh(t, u) \leq \beta u^2 \tag{16}$$

for all (t, u), where α and β are real numbers with $\beta \geq \alpha$, then h belongs to the sector $[\alpha, \beta]$. If $h(t, u)$ belongs to the sector $[0, \infty]$, that is, $uh(t, u) \geq 0$, then the system $y = h(t, u)$ is passive. If $h(t, u)$ belongs to the sector $(0, \infty)$, then $y = h(t, u)$ is strictly passive.

3.2.2. Strictly Positive Real Transfer Functions. A single-input–single-output linear system transfer function $G(s)$ is strictly positive real function if and only if

(1) $G(\infty) > 0$,

(2) all poles of $G(s)$ are in $\mathrm{Re}[s] < 0$, and

(3) $\mathrm{Re}[G(j\omega)] > 0, \forall \omega > 0$.

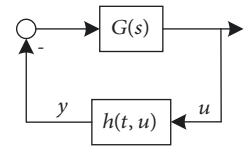

Figure 7: Feedback connection.

The second condition requires all poles of $G(s)$ to be in the open left-half complex plane, whereas the third condition requires the Nyquist plot of $G(j\omega)$ to lie in the closed right-half complex plane.

Lemma 1 provides the relationship between positive real and passivity properties.

Lemma 1. *The linear time-invariant minimal realization*

$$\begin{aligned} \dot{x} &= Ax + Bu \\ y &= Cx + Du \end{aligned} \tag{17}$$

with $G(s) = C(sI - A)^{-1}B + D$ is strictly passive if $G(s)$ is strictly positive real function.

3.2.3. Passivity Theorems. Consider the feedback connection of Figure 7, where $G(s)$ is a time-invariant dynamical system and $h(t, u)$ is a time-varying memoryless function. Theorem 2 presents the method of analyzing the Lyapunov stability of feedback systems; this method uses the passivity properties of the feedback components.

Theorem 2. *Consider the feedback connection of a strictly passive, time-invariant, dynamical system $G(s)$ with a passive, time-varying, memoryless function $h(t, u)$. Then, the origin of the closed-loop system is uniformly asymptotically stable.*

Furthermore, if $G(s)$ is a strictly positive real transfer function (from Lemma 1), then the dynamical system is strictly passive. According to Theorem 2, the origin of the closed-loop system is uniformly asymptotically stable.

3.2.4. Loop Transformations. When $G(s)$ or $h(t, u)$ does not satisfy the conditions of Theorem 2, the feedback system can be transformed into an equivalent feedback system, which satisfies the conditions through loop transformations. Suppose $G(s)$ is a time-invariant dynamical system and $h(t, u)$ is a time-varying memoryless function that belongs to the sector $[\alpha, \beta]$. Then, the feedback system can be reconfigured into a feedback system that is connected by $\widetilde{G}(s)$ and $\widetilde{h}(t, u)$ through loop transformations, as shown in Figure 8, where $\widetilde{h}(t, u)$ is a memoryless function that belongs to the sector $[0, \infty]$. We can now apply Theorem 2 if $\widetilde{G}(s)$ satisfies the conditions of the respective theorem. In this case, the systems shown in Figures 7, 8(a), and 8(b) are equivalent in terms of stability.

4. Stability Analysis of the Guidance System

The guidance system shown in Figure 6 is transformed into a feedback system, as shown in Figure 7, wherein the

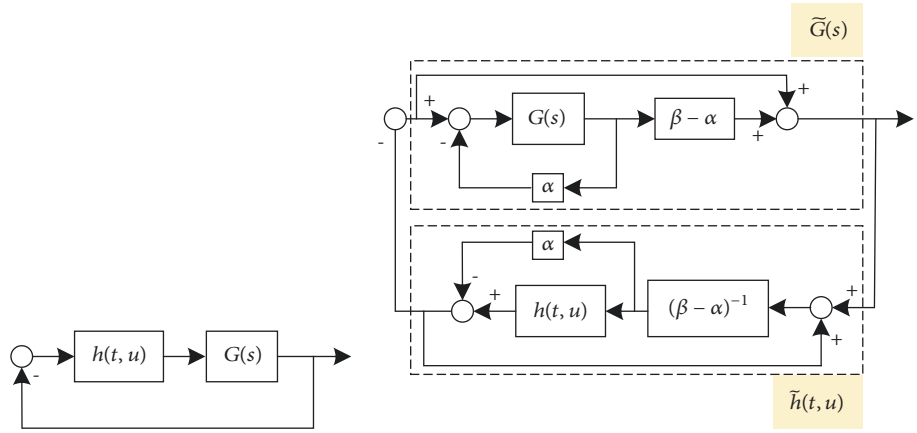

(a) Equivalent system (b) Loop transformations

Figure 8: Bock diagrams of equivalent feedback system.

linear time-invariant system transfer function is as follows:

$$G(\bar{s}) = \frac{N}{\bar{s}\left[(\bar{s}/5+1)^4 - N\left(V_c/V_m\right)R(\bar{s})\left(\overline{T}_\alpha \bar{s}+1\right)\right]}, \quad (18)$$

whereas the time-varying memoryless function is as follows:

$$h(\bar{t}, u) = \frac{1}{\overline{T}_F - \bar{t}}. \quad (19)$$

Let $\bar{t}_k$ be any moment of the terminal guidance. We discuss the stability of guidance systems in the bounded closed domain $\bar{t} \in [0, \bar{t}_k]$. Then, $h(\bar{t}, u)$ belongs to the sector $[1/\overline{T}_F, 1/(\overline{T}_F - \bar{t}_k)]$ and is not passive. With the use of transformations to reconfigure the system into the form shown in Figure 8(b), where $\tilde{h}(\bar{t}, u)$ is a time-varying memoryless function that belongs to the sector $[0, \infty]$, $G(\bar{s})$ is transformed into

$$\widetilde{G}(\bar{s}) = \frac{\bar{s}\left[(\bar{s}/5+1)^4 - N\left(V_c/V_m\right)R(\bar{s})\left(\overline{T}_\alpha \bar{s}+1\right)\right] + N/\left(\overline{T}_F - \bar{t}_k\right)}{\bar{s}\left[(\bar{s}/5+1)^4 - N\left(V_c/V_m\right)R(\bar{s})\left(\overline{T}_\alpha \bar{s}+1\right)\right] + N/\overline{T}_F}. \quad (20)$$

In accordance with Theorem 2, if $\widetilde{G}(\bar{s})$ is strictly positive real, then the feedback system satisfies the Lyapunov stability condition; that is, the origin of the original PN guidance system is uniformly asymptotically stable over the $\bar{t} \in [0, \bar{t}_k]$ interval. The following are three conditions for $\widetilde{G}(\bar{s})$ to be strictly positive real:

(i) Substituting the DRRTF in Table 1 into (14) shows that $\widetilde{G}(\infty) = 1 > 0$ for each DRRTF. Therefore, the first condition is satisfied.

(ii) Expanding the characteristic equation of $\widetilde{G}(\bar{s})$ into the following form:

$$a_n s^n + a_{n-1} s^{n-1} + \cdots + a_2 s^2 + a_1 s^1 + a_0 = 0 \quad (21)$$

Then, for the second condition, the Routh criterion can be used to obtain the constraint inequality that the eigenvalues are all on the open left-half complex plane.

(iii) The third condition holds when the Nyquist plot of $\widetilde{G}(j\bar{\omega})$ lies in the closed right-half complex plane.

The previous analysis shows that the parameters that affect the stability of the PN guidance system include N, V_c/V_m, $\overline{T}_\alpha$, $\overline{T}_F$, $\bar{t}_k$, and $R(\bar{s})$.

5. Simulations and Analysis

This section analyzes the influence of different DRRTF models caused by disturbance torque and radome error on the stability of the guidance system through simulations. The typical PN guidance system parameters ($N = 4$, $V_c/V_m = 1.5$, $\overline{T}_\alpha = 3$, $\overline{T}_F = 10$, and $T_g = 0.5$), equivalent gains ($K_1 = 10$, $K_2 = 10$), and disturbance torque coefficients ($K_n = 0.001$, $K_\omega = 0.001$) are selected. In accordance with the Routh criterion, the second condition under the abovementioned parameters is satisfied. To examine the third condition, take K_r equal to −0.03 and 0.03, respectively, and the Nyquist plots of $\widetilde{G}(j\bar{\omega})$ corresponding to different DRRTF models and $\bar{t}_k$ are presented in Figure 9.

Figure 9 illustrates that the critical stability time $\bar{t}_{kc}$ for different DRRTF models is different under the same conditions. Regardless of the disturbance torque type, the critical stability time of the system when $K_r = 0.03$ is greater than that when $K_r = -0.03$. Therefore, when $K_r = -0.03$, the constraint on the terminal guidance time when the guidance system satisfies the Lyapunov stability conditions is stricter than that when $K_r = 0.03$.

$\bar{t}_{uns} = \overline{T}_F - \bar{t}_k$ indicates unstable flight time. Figure 10 shows the uniformly asymptotically stable boundary of the system determined by K_s or K_v and $\bar{t}_{uns}$ under different $\overline{T}_F$ when $N = 4$ and $\overline{T}_\alpha = 3$. The regions above and below the curve are stable and unstable, respectively.

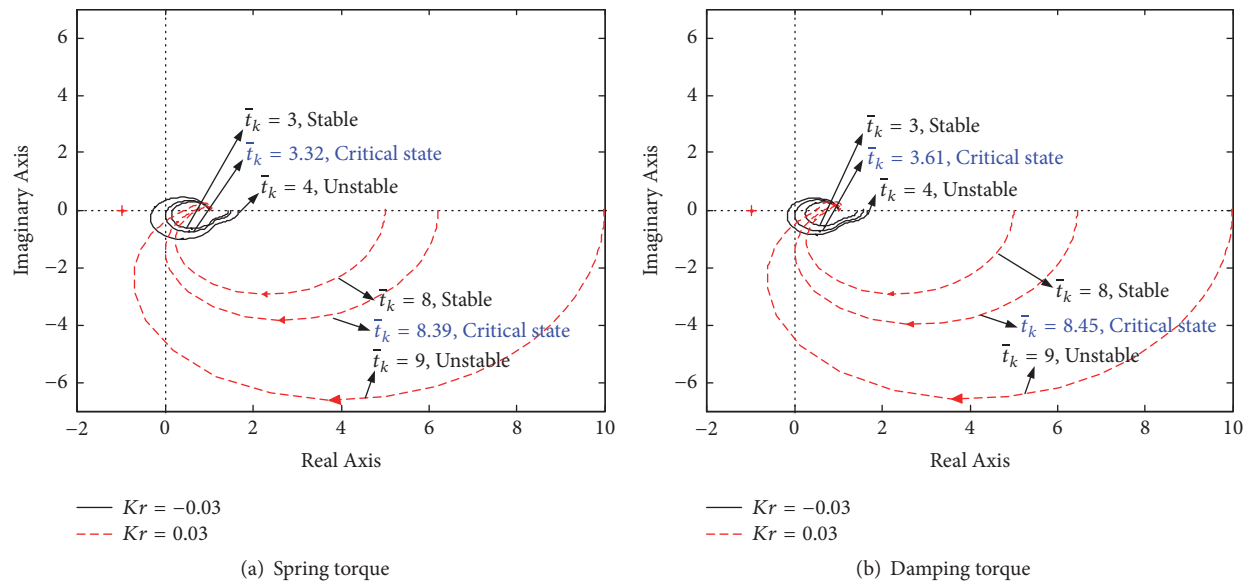

(a) Spring torque (b) Damping torque

Figure 9: Nyquist plots.

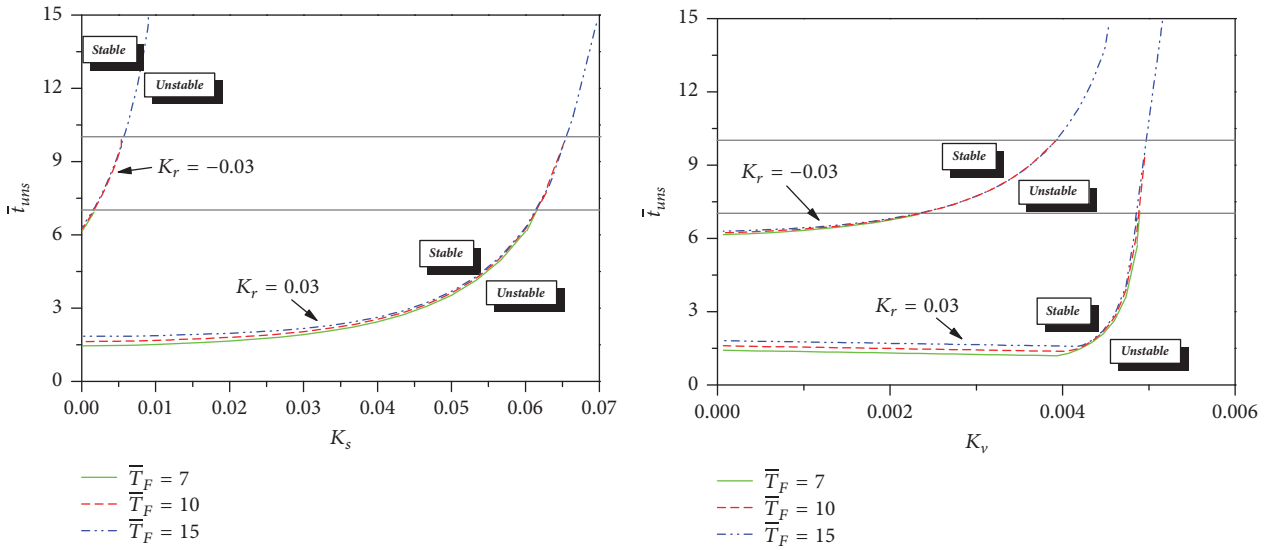

(a) Spring torque (b) Damping torque

Figure 10: Stable boundary corresponding to different $\bar{T}_F$.

Figure 10 illustrates that different $\bar{T}_F$ have little effect on the unstable flight time of the guidance system. The time of instability can be delayed by extending the terminal guidance time. Under the action of spring torque, the unstable flight time $\bar{t}_{uns}$ increases rapidly with the increase of K_s. When K_s increases to a certain value, the guidance system cannot meet the stability conditions during the entire terminal guidance time. Moreover, when $K_r = -0.03$, the unstable flight time is higher and the stability regions are smaller than those when $K_r = 0.03$. The change law of the stable boundary of the guidance system under the action of the damping moment is similar to that of the spring torque. Only when $K_r = 0.03$, the unstable flight time decreases slightly and then increases rapidly with the increase of K_v.

Figure 11 shows the uniformly asymptotically stable boundary of the system determined by K_r and $\bar{t}_{uns}$ under different disturbances when $\bar{T}_F = 10$.

Figure 11 illustrates that when $K_r < 0$, the unstable flight time is considerably larger than that when $K_r > 0$ and increases sharply with the increase of $|K_r|$. When $K_r < 0$, the tolerance of the guidance system to the radome error is approximately 3%, which is less than that when $K_r > 0$ (higher than 8%). When $K_r > 0$, the unstable flight time decreases slowly as $|K_r|$ increases, which is beneficial to

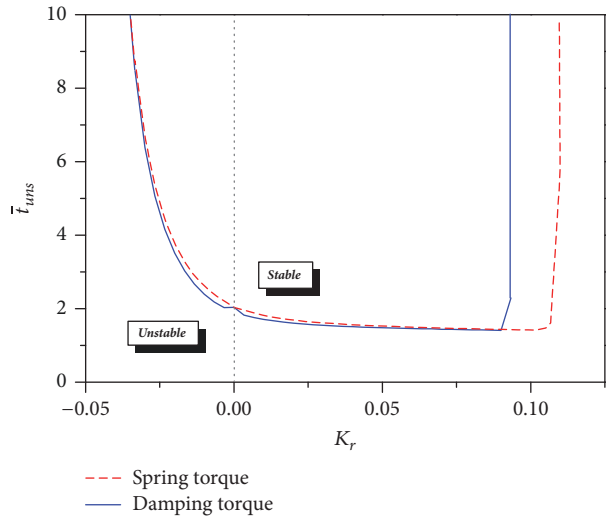

FIGURE 11: Stable boundary corresponding to different K_r.

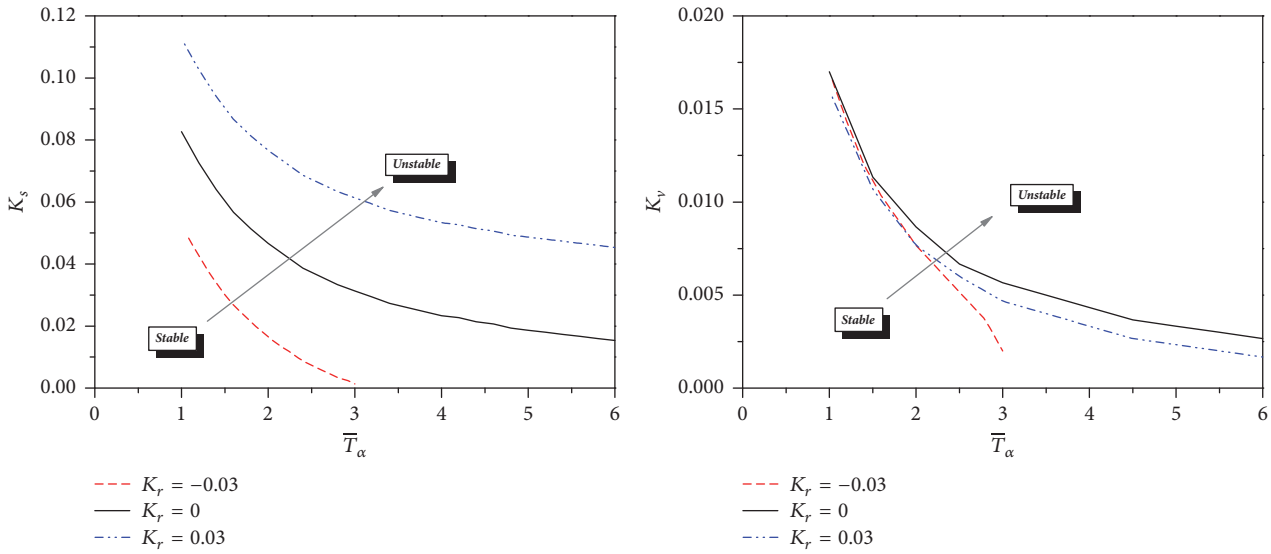

(a) Spring torque

(b) Damping torque

FIGURE 12: Stable boundary corresponding to different $\overline{T}_\alpha$.

the guidance system. However, when $|K_r|$ exceeds a certain limit, the guidance system immediately becomes unstable, indicating that the tolerance of the guidance system to the radome error is also limited.

Figure 12 presents the uniformly asymptotically stable boundary of the system determined by $\overline{T}_\alpha$ and K_s or K_v under different K_r when $\overline{T}_F = 10$ and $\bar{t}_{uns} = 7$.

Figure 12 shows that the stability regions of the guidance system decrease with the increase of $\overline{T}_\alpha$. $\overline{T}_\alpha$ is related to the altitude of the missile's flight, and $\overline{T}_\alpha$ is relatively large at high altitude. If T_g is small, then the guidance system will likely lose stability when the missile is flying at a high altitude. Therefore, the decelerating response of the guidance system in high airspace should be given considerable attention. Moreover, under the action of spring torque, the stability regions when $K_r < 0$ are smaller and the stability regions when $K_r > 0$ are larger than that when $K_r = 0$. Under the action of damping torque, positive and negative K_r lead to a stability regions reduction. When K_r decreases to a certain value and $\overline{T}_\alpha$ is large, the guidance system will not be stable. Therefore, the disturbance rejection rate index should be strictly constrained in engineering practice.

From the above analysis, the stability regions for a negative slope are smaller than that for a positive slope, and lager values of $\overline{T}_\alpha$ lead to a smaller range of stability. These trends are consistent with those obtained in [8] using the Routh criterion. However, there will be differences in the stability margin.

6. Conclusions

The influence of the disturbance rejection rate and radome error slope on the Lyapunov stability of the PN guidance system is analyzed by passivity theorems. Results of the simulation show that different DRRTF models have different effects on the stability of the guidance system. The stable boundary and tolerance of the PN guidance system to the spring torque, damping torque, and radome slope differ significantly. The unstable flight time caused by negative radome slope is higher than that due to positive radome slope. The constraint of disturbance rejection rate index when the radome slope is negative and is stricter than that when radome slope is positive. These results provide a theoretical basis for the overall design and engineering application of guidance systems and radar seekers.

Data Availability

The data used to support the findings of this study (in txt format) are available from the corresponding author upon request.

Conflicts of Interest

The authors declare that there are no conflicts of interest regarding the publication of this paper.

References

[1] P. J. Kennedy and R. L. Kennedy, "Direct versus indirect line of sight (LOS) stabilization," *IEEE Transactions on Control Systems Technology*, vol. 11, no. 1, pp. 3–15, 2003.

[2] Y. S. Kwon, H. Y. Hwang, and Y. S. Choi, "Stabilization loop design on direct drive gimbaled platform with low stiffness and heavy inertia," in *Proceedings of the International Conference on Control, Automation and Systems (ICCAS '07)*, pp. 320–325, IEEE, Seoul, South Korea, October 2007.

[3] S. Mondal, S. Sadhu, and A. Banerjee, "Platform motion disturbances attenuation in a missile seeker subsystem using Internal Model Control," in *Proceedings of the 2013 IEEE International Conference on Control, Automation, Robotics and Embedded Systems, CARE 2013*, ind, December 2013.

[4] I. Klein and I. Rusnak, "Loop-shaping approach to mitigate radome effects in homing missiles," *Journal of Guidance, Control, and Dynamics*, vol. 40, no. 7, pp. 1787–1793, 2017.

[5] S. S. Han, S. K. Jang, and S. J. Lee, "Radome compensation using adaptive particle filter," in *Proceedings of the 17th IFAC Symposium on Automatic Control in Aerospace, ACA' 2007*, pp. 43–48, fra, June 2007.

[6] C.-L. Lin and Y.-H. Hsiao, "Adaptive feedforward control for disturbance torque rejection in seeker stabilizing loop," *IEEE Transactions on Control Systems Technology*, vol. 9, no. 1, pp. 108–121, 2001.

[7] S. Mondal, S. Sadhu, and S. Talukdar, "Platform motion disturbances attenuation in a missile seeker subsystem using disturbance observer techniques," in *Proceedings of the 10th International Conference on Intelligent Systems and Control, ISCO 2016*, ind, January 2016.

[8] F. W. Nesline and P. Zarchan, "Radome induced miss distance in aero-dynamically controlled homing missiles," in *Proceedings of the Collection of Technical Papers - AIAA Guidance and Control Conference*, 1984, pp. 1984-1845.

[9] P. Zarchan, *Tactical and Strategic Missile Guidance*, AIAA, Reston, Va, USA, 2012.

[10] J. Song, G. Cai, L. Kong, and J. Fan, "Precision analysis of the semi-strapdown homing guided system," *Journal of Aerospace Engineering*, vol. 27, no. 1, pp. 151–167, 2014.

[11] Y. Du, Q. Xia, and Z. Wang, "Effect of seeker disturbance rejection performance on the control system stability," in *Proceedings of the 3rd International Symposium on Systems and Control in Aeronautics and Astronautics, ISSCAA2010*, pp. 1032–1035, chn, June 2010.

[12] H. Eguchi, H. Kubo, and T. Yamashita, "Robust stability of guidance and control system for homing missiles," in *Proceedings of the 29th Aerospace Sciences Meeting*, Reno, NV, USA, 1991.

[13] O. Goldan and S. Gutman, "Adjoint stability and miss distance in proportional navigation," *Journal of Guidance, Control, and Dynamics*, vol. 35, no. 4, pp. 1089–1093, 2012.

[14] M. Guelman, "The stability of proportional navigation systems," in *Proceedings of the Guidance, Navigation and Control Conference*, pp. 586–590, usa, August 1990.

[15] P. Gurfil, M. Jodorkovsky, and M. Guelman, "Finite time stability approach to proportional navigation systems analysis," *Journal of Guidance, Control, and Dynamics*, vol. 21, no. 6, pp. 853–861, 1998.

[16] D.-Y. Rew, M.-J. Tahk, and H. Cho, "Short-time stability of proportional navigation guidance loop," *IEEE Transactions on Aerospace and Electronic Systems*, vol. 32, no. 3, pp. 1107–1115, 1996.

[17] T. Tanaka and H. Eguchi, "Hyperstable range in homing missiles," in *Proceedings of the Guidance, Navigation and Control Conference, 1990*, pp. 591–600, usa, August 1990.

[18] S. Jianmei, C. Gaohua, C. Xianxiang, and K. Lixia, "Stability region analysis of the parasitic loop of the semi-strapdown homing seeker," *Proceedings of the Institution of Mechanical Engineers, Part I: Journal of Systems and Control Engineering*, vol. 226, no. 4, pp. 550–562, 2012.

[19] H. K. Khalil, *Nonlinear Systems Third Edition*, Prentice-Hall, Inc, Upper Saddle River, NJ, 2002.

[20] C. I. Byrnes, A. Isidori, and J. C. Willems, "Passivity, feedback equivalence, and the global stabilization of minimum phase nonlinear systems," *Institute of Electrical and Electronics Engineers Transactions on Automatic Control*, vol. 36, no. 11, pp. 1217–1240, 1991.

[21] A. Teel et al., "Input-output stability," in *The Control Handbook*, p. 4250, CRC Press, 1995.

[22] X. Du and Q. Xia, "The research of guidance performance of the phased array seeker with platform for air-to-air missile," *Optik - International Journal for Light and Electron Optics*, vol. 127, no. 22, pp. 10322–10334, 2016.

[23] F. W. Nesline and M. L. Nesline, "Wing size vs radome compensation in aerodynamically controlled radar homing missiles," *Journal of Guidance, Control, and Dynamics*, vol. 9, no. 6, pp. 645–649, 1986.

[24] P. Zarchan and H. Gratt, "Adaptive radome compensation using dither," *Journal of Guidance, Control, and Dynamics*, vol. 22, no. 1, pp. 51–57, 1999.